Structure *14*, 1377–1388, September 2006 ©2006 Elsevier Ltd All rights reserved DOI 10.1016/j.str.2006.07.001

Crystal Structure of Ethylbenzene Dehydrogenase from *Aromatoleum aromaticum*

Daniel P. Kloer,[1] Corina Hagel,[2] Johann Heider,[2] and Georg E. Schulz[1,*]
[1] Institut für Organische Chemie und Biochemie
Albert-Ludwigs-Universität
Albertstr. 21
D-79104 Freiburg im Breisgau
Germany
[2] Fachbereich Biologie
Institut für Mikrobiologie und Genetik
Schnittspahnstr. 10
D-64287 Darmstadt
Germany

Summary

Anaerobic degradation of hydrocarbons was discovered a decade ago, and ethylbenzene dehydrogenase was one of the first characterized enzymes involved. The structure of the soluble periplasmic 165 kDa enzyme was established at 1.88 Å resolution. It is a heterotrimer. The α subunit contains the catalytic center with a molybdenum held by two molybdopterin-guanine dinucleotides, one with an open pyran ring, and an iron-sulfur cluster with a histidine ligand. During catalysis, electrons produced by substrate oxidation are transferred to a heme in the γ subunit and then presumably to a separate cytochrome involved in nitrate respiration. The β subunit contains four iron-sulfur clusters and is structurally related to ferredoxins. The γ subunit is the first known protein with a methionine and a lysine as axial heme ligands. The catalytic product was modeled into the active center, showing the reaction geometry. A mechanism consistent with activity and inhibition data of ethylbenzene-related compounds is proposed.

Introduction

Ethylbenzene dehydrogenase (EBDH, EC 1.17.99.2) was isolated from *Aromatoleum aromaticum* strain EbN1 (formerly named *Azoarcus* sp.). The strain was derived from freshwater mud after anaerobic cultivation on crude oil in the presence of nitrate, demonstrating that aromatic hydrocarbons can be degraded anaerobically (Rabus and Widdel, 1995). Furthermore, it was shown that the enzyme EBDH catalyzes the dioxygen-independent stereospecific hydroxylation of ethylbenzene to 1-(*S*)-phenylethanol, which is the first step of the degradation pathway (Kniemeyer and Heider, 2001; Johnson et al., 2001). EBDH contains molybdenum and is a soluble periplasmic protein. It couples to artificial electron acceptors only if they have a high redox potential, like the ferricenium ion with an $E^{0\prime}$ of +380 mV. This suggests that its natural electron acceptor may be a periplasmic cytochrome c of similarly high potential. The free energy corresponding to the large redox potential difference between the electron acceptor and the 1-phenylethanol/ethylbenzene couple with an $E^{0\prime}$ of +30 mV is dissipated, explaining the observed irreversibility of the reaction (Kniemeyer and Heider, 2001).

Sequence comparisons indicated that EBDH is a member of the dimethylsulfoxide (DMSO) reductase family of molybdenum *bis*-molybdopterin-guanine dinucleotide (Mo-*bis*MGD) enzymes, which together with the xanthine oxidase and sulfite oxidase families comprise all known enzymes with mononuclear molybdenum in the active center (Hille, 1996). The members of the DMSO reductase family are from bacterial and archaeal species and seem to be more numerous than those of the other two families. The DMSO family has been subdivided into subfamilies I, II, and III (McDevitt et al., 2002). The initial structure of a subfamily I member was that of formate dehydrogenase-H (Boyington et al., 1997). The first structures of subfamily II and III members were those of a respiratory nitrate reductase NarGHI (Bertero et al., 2003; Jormakka et al., 2004) and of DMSO reductase (Schindelin et al., 1996), respectively.

EBDH is a heterotrimer and belongs to subfamily II (Johnson et al., 2001). In contrast to the other structurally known member of subfamily II, the membrane bound nitrate reductase NarGHI, EBDH is soluble and located in the periplasm. It has been shown that its α subunit contains the cofactor Mo-*bis*MGD and one Fe-S cluster, while its β subunit carries several Fe-S clusters and its γ subunit binds a heme b (Fe-protoporphyrin IX) (Kniemeyer and Heider, 2001; Johnson et al., 2001; Szaleniec et al., 2003). The isolated enzyme is unstable in an aerobic environment but can be stabilized by the addition of a strong oxidant with an $E^{0\prime}$ of around +400 mV, presumably because the oxidant keeps heme b in its ferric state preventing oxygen radical production. Here, we report the high-resolution structure of EBDH, establishing the conformations of the α, β, and γ subunits together with the stoichiometry and structure of the cofactors and their mode of assembly.

Results

Structure Determination

The EBDH crystals belonged to space group $P2_1$ with one heterotrimeric molecule in the asymmetric unit. Since EBDH was known to contain several Fe-S clusters in the α and β subunits (Kniemeyer and Heider, 2001; Johnson et al., 2001), data were collected at the iron K edge to maximize the anomalous signal for phasing. Unfortunately, the long X-ray wavelength caused considerable radiation damage so that successive data sets from the same crystal showed R_{iso} values as high as 15%, which prevented phasing by multiwavelength methods. Using an attenuated beam, however, we succeeded in collecting a suitable data set at the iron peak wavelength and used it for single wavelength anomalous diffraction (SAD) phasing (Table 1).

At 6 Å resolution, the anomalous differences revealed six scatterers. Later on, it turned out that they represented the iron atoms of five Fe-S clusters and heme b.

*Correspondence: georg.schulz@ocbc.uni-freiburg.de

Table 1. X-Ray Data Collection and Refinement Statistics

Data Collection[a]		
Data set	High resolution	SAD
Wavelength (Å)	1.2400	1.7381
Resolution[b] (Å)	50–1.88 (1.94–1.88)	50–2.4 (2.6–2.4)
Unique reflections	127,864	116,641[c]
Completeness[b] (%)	98.0 (80.7)	91.1 (58.8)
Average I/σ(I)[b]	8.8 (2.8)	9.7 (2.7)
R_{merge}[b] (%)	10.4 (38.5)	13.6 (46.7)
Multiplicity	3.6	5.9[c]

Refinement[a]	
Resolution range (Å)	47–1.88
Unique reflections	127,864
Protein atoms	11,571
Cofactors and ligands	250
Water molecules	818
Average *B*-factors (Å^2)[d]	24.8
Main chain	
Cofactors and acetate	19.8
Water molecules	35.6
RMSD bond lengths (Å)/angles (deg.)	0.016/1.64
R_{cryst} (%)/R_{free} (5% test set) (%)	14.8/18.3
Ramachandran statistics Favored (%)	97.4
Allowed (%)	2.5
Disallowed (%)	0.1

[a] The crystals belonged to space group $P2_1$ with one heterotrimeric EBDH molecule per asymmetric unit. The unit cell parameters were a = 112.5 Å, b = 67.3 Å, c = 114.8 Å, β = 111.3° for the crystal measured to high resolution and a = 113.9 Å, b = 68.4 Å, c = 116.7 Å, β = 111.7° for the crystal used for the SAD measurement. The solvent content was 50%. All data were collected at 100 K.
[b] The values in parentheses refer to the outermost shell.
[c] Friedel pairs treated as separate reflections.
[d] Residual *B*-factors after TLS refinement. One TLS group was used for each subunit together with its bound cofactors.

Since the individual iron atoms of the clusters could not be resolved, the phases were calculated only at low resolution and subsequently improved by density modification. This yielded a 4.2 Å resolution map showing numerous α helices. The model was then improved by a molecular replacement procedure based on the homologous α and β subunits NarG and NarH of respiratory nitrate reductase (Bertero et al., 2003). The reductase was positioned onto the five recognized Fe-S clusters and those parts of the reductase that fitted the 4.2 Å resolution density of EBDH were used as a partial model. The phases of this partial model were then combined with the experimental 4.2 Å phases to yield further pieces of the structure. After several iterations, the phases were extended to the full 1.88 Å resolution of the data set, and a complete model was built and refined to good quality indices (Table 1).

Oligomeric Structure

The subunit organization of the EBDH heterotrimer is shown in Figure 1. The overall shape is that of a "horn of plenty." The opening of the horn is formed by the α subunit, which contains the active center with a Mo-*bis*MGD cofactor and one Fe-S cluster (FS0). The remaining four Fe-S clusters FS1 through FS4 are in the β subunit functioning as an electron transport chain to the heme b of the γ subunit at the tip of the horn. The direct distance between molybdenum and the heme iron is 64 Å. The γ subunit most likely communicates with a terminal electron acceptor that has not yet been identified. The α and β subunits are tightly associated, showing a contact area of 4395 Å^2, while the interface between the β and γ subunits is merely 983 Å^2.

The oligomer architecture of the EBDH heterotrimer is similar to that of the respiratory nitrate reductase NarGHI (Bertero et al., 2003; Jormakka et al., 2004) and formate dehydrogenase-N (Jormakka et al., 2002) both of which, however, are membrane bound and form dimers of heterotrimers, i.e., hexamers. The α and β subunits of all three enzymes are homologous. However, the γ subunit of EBDH differs completely from those of the other two enzymes. Other structures related to the α, β, and γ subunits are listed in Table 2.

The α Subunit

After removal of a signal peptide of the twin-arginine-transport (tat) type (Rabus et al., 2002), the crystallized polypeptide starts at position 55. In the crystal, the chain is visible from Glu65 to Ala976. Residues 65–74 are associated with the β subunit, whereas residues 55–64 are mobile. The α subunit harbors the active center with its Mo-*bis*MGD cofactor system, the chemical structure of which is shown in Figure 2. The two MGD molecules differ from each other in that one has a closed pyran ring, while the other assumes an open form. As usual (Hille, 2002), the Mo ion is held by two dithiolene groups. In addition, the subunit contains one [4Fe-4S] cluster named FS0. The structure around the Mo ion is documented in Figure 3. The electron density shows clearly the open pyran ring of MGD-P and the closed ring of MGD-Q. Such an open MGD molecule was also observed in one of the two NarG structures (Bertero et al., 2003) and could not be excluded in the other (Jormakka et al., 2004). The open form of MGD-P is stabilized by hydrogen bonds between the 3′-hydroxyl group and His855-Nδ as well as Arg612-Nζ. It is far away from the first cluster FS0 and therefore unlikely to be involved in electron transfer. The corresponding ring oxygen of the closed MGD-Q is in a less polar environment.

The chemical structure at the ring atoms C6 and C7 of the open MGD-P is not yet clarified. However, our electron density in Figure 3 clearly indicated a flat sp2 center at C6, favoring the tautomer drawn out in Figure 2. This finding contradicts the reported tetrahedral C6 atom of the open MGD-P of NarG (Bertero et al., 2003). It should be noted that our electron density is also consistent with a third double bond in the piperazine ring rendering it aromatic. Such a conversion would involve an oxidation in the neighborhood of the Mo redox center, which is quite conceivable. The stereo centers of the C4a and C10a atoms of the closed MGD-Q were derived from the electron density and stated explicitly in Figure 2 because they were not always assigned in recent publications.

Surprisingly, the long α chain of 912 structured residues does not form domains separated along the chain. Following previous publications (Boyington et al., 1997; Schindelin et al., 1996), we defined domain I (residues 65–138, 659–676, and 737–770) containing cluster FS0, domain II (146–222, 486–652, and 687–728) binding the open MGD-P, domain III (226–468 and 777–824) binding the closed MGD-Q, and domain IV (843–976), as shown

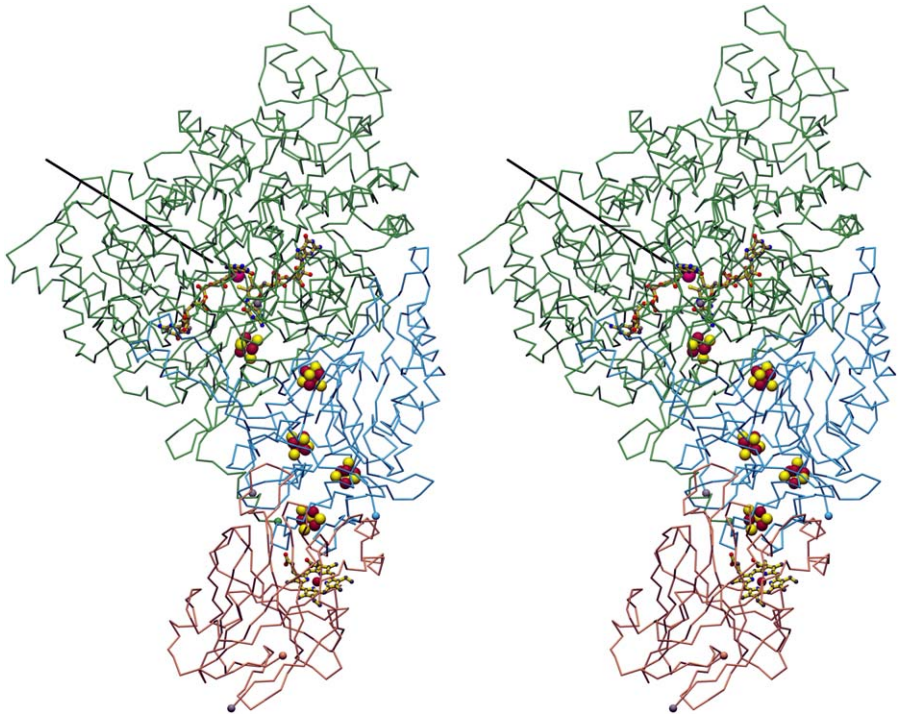

Figure 1. Stereoview of the Heterotrimeric EBDH

The Cα backbones of the α, β, and γ subunits are shown in green, blue, and orange, respectively. The N termini are appropriately colored spheres, and the C termini are gray spheres. Mo-*bis*MGD, the iron-sulfur clusters, and the heme are depicted in an atomic representation. All cofactors are part of an electron transport chain traversing all three subunits. The tunnel-like pocket leading to the active center is marked by a black line. During catalysis, two electrons resulting from the use of water for the hydroxylation of ethylbenzene are transferred from the Mo center in the α subunit to the heme iron in the γ subunit, from where they are donated to a yet-unknown acceptor.

in different colors in Figure 4A. This assignment follows the spatial locations so that the domains are not separable along the chain and therefore unlikely to represent general building blocks transferred from protein to protein during evolution. However, two comparatively small βαβαβ-Rossmann motifs are present in domains II and III (Figure 4A), binding the two MGD dinucleotides in the commonly observed geometry (Schulz, 1992).

A deep pocket extends from the opening of the "horn of plenty" to the active center of EBDH in the interior of the α subunit (Figure 1). Since it is lined with predominantly nonpolar residues containing only few crystallographically defined water molecules, it is well suited for the passage of nonpolar substrates such as ethylbenzene. The [4Fe-4S] cluster FS0 of the α subunit is of the usual type except for one of the four iron ligands being a histidine instead of a cysteine, as observed with NarGHI (Bertero et al., 2003). It is at a suitable electron transfer distance from the pterin moiety of the closed MGD-Q.

A search for structures resembling the α subunit of EBDH revealed the α subunit of the respiratory nitrate reductase NarG (Bertero et al., 2003; Jormakka et al., 2004) as the closest homolog showing 723 equivalent Cα atoms within the usual 3 Å cut-off criterion (Table 2). Further structural homologs are DMSO reductases (Schindelin et al., 1996; McAlpine et al., 1998), pyrogallol-phloroglucinol transhydroxylase (Messerschmidt et al., 2004), Mo-containing formate dehydrogenases (Boyington et al., 1997; Jormakka et al., 2002), a tungsten-containing formate dehydrogenase (Raaijmakers et al., 2002), the nitrate reductase NapA (Dias et al., 1999; Arnoux et al., 2003) and arsenite oxidase (Ellis et al., 2001), which show 598 to 444 equivalenced Cα atoms within the cut-off criterion. This indicates significant evolutionary relationships, in particular in view of the entangled chainfold of the α subunit.

The β Subunit

The structured part of this subunit consists of residues 16–352 (Figure 4B). The 15 N-terminal residues are disordered. Interestingly, both N termini of the α and β subunits are disordered and located in the same region of the enzyme showing a distance of 19 Å between the first ordered Cα atoms. It is conceivable that these mobile chain ends are important for anchoring EBDH in a particular subcellular region.

The β subunit contains four of the five iron-sulfur clusters of EBDH. Together with FS0 from the α subunit, these clusters are arranged in a "W" shape (Figure 1). The four clusters of the β subunit can be considered as two cluster pairs related to each other by a pseudo 2-fold axis. The chainfold of each part is closely related to the seven-iron type of ferredoxins (Macedo-Ribeiro et al., 2001). Actually the β subunit can be considered as an N-terminal ferredoxin (green) followed in tandem by a duplication (red) starting at strand β11 shown in Figure 4B. We suggest that such a duplication occurred during evolution and was then followed by a swap of strands β10 (green) and β14 (red) together with their respective preceding peptide.

A sketch of the tandem is shown in Figure 5A. The close spatial relationship between these two parts of

Table 2. Structural Comparisons

Enzyme, Source, Reference[a]	Oligomer Organization	Compared Subunit	Mo Ligand	Subfamily	Structure of *bis*MGD[b]	4Fe-4S Clusters	Other Cofactors	Aligned Residues	Identical Resid. (%)	Chain Length
EBDH, *A. aromaticum* (1)	$\alpha\beta\gamma$	α	Oδ2	II	c - o	1	—	—	—	912
NarG, nitrate reductase, *E. coli* (2)	$(\alpha\beta\gamma')_2$	α	Oδ1, Oδ2	II	c - o	1	—	723	26	1244
NarG, nitrate reductase, *E. coli* (3)	$(\alpha\beta\gamma')_2$	α	Oδ2	II	c - c	1	—	723	26	1244
DMSO reductase, *R. sphaeroides* (4)	α	α	Oγ	III	c - c	—	—	598	20	767
DMSO reductase, *R. capsulatus* (5)	α	α	Oγ	III	c - c	—	—	504	22	823
TMAO reductase, *S. massilia* (6)	α	α	Oγ	III	c - c	—	—	444	13	794
Pyr-phlo transhydroxyl., *P. acidigalli* (7)	$\alpha\beta$	α	Oγ	III	c - c	—	—	533	22	875
Formate dehydrogenase-N, *E. coli* (8)	$(\alpha\beta\gamma')_2$	α	Seγ	I	c - c	1	—	514	18	982
Formate dehydrogenase-H, *E. coli* (9)	α	α	Seγ	I	c - c	1	—	446	18	697
W-formate dehydrogenase, *D. gigas* (10)	$\alpha\beta$	α	Seγ	I	c - c	1	—	509	19	977
NapA, nitrate reductase, *D. desulfuricans* (11)	α	α	Sγ	I	c - c	1	—	464	19	720
NapA, nitrate reductase, *R. sphaeroides* (12)	$(\alpha\beta')_2$	α	Sγ	I	c - c	1	—	484	18	789
Arsenite oxidase, *A. faecalis* (13)	$(\alpha\beta')_2$	α	OH^-	—	c - c	—	3Fe-4S	479	17	822
EDBH, *A. aromaticum* (1)	$\alpha\beta\gamma$	β	—	—	—	3	3Fe-4S	—	—	337
NarH, nitrate reductase, *E. coli* (2)	$(\alpha\beta\gamma')_2$	β	—	—	—	3	3Fe-4S	290	46	509
Pyr-phlo transhydroxyl., *P. acidigalli* (7)	$\alpha\beta$	β	—	—	—	3	—	165	32	274
Formate dehydrogenase-N, *E. coli* (8)	$(\alpha\beta\gamma')_2$	β	—	—	—	4	—	161	30	294
W-formate dehydrogenase, *D. gigas* (10)	$\alpha\beta$	β	—	—	—	3	—	149	26	214
EBDH, *A. aromaticum* (1)	$\alpha\beta\gamma$	γ	—	—	—	—	heme b	—	—	214
Xylanase 10A, *T. maritima* (14)	—	C2	—	—	—	—	—	124	12	189
Cellobiose dehydr., *P. chrysosporium* (15)	—	cyt	—	—	—	—	heme b	96	7	186
Fab fragment, *M. musculus* (16)	—	V_H	—	—	—	—	—	75	7	120

[a] Protein Data Bank accession codes and references: (1) 2IVF; (2) 1Q16 (Bertero et al., 2003); (3) 1R27 (Jormakka et al., 2004); (4) 1EU1 (Schindelin et al., 1996); (5) 4DMR (Schneider et al., 1996; McAlpine et al., 1998); (6) 1TMO (Czjzek et al., 1998); (7) 1VLD (Messerschmidt et al., 2004); (8) 1KQF (Jormakka et al., 2002); (9) 1AA6 (Boyington et al., 1997); (10) 1H0H, the enzyme contains tungsten instead of molybdenum (Raaijmakers et al., 2002); (11) 2NAP (Dias et al., 1999); (12) 1OGY (Arnoux et al., 2003); (13) 1G8K (Ellis et al., 2001); (14) 1I82, carbohydrate binding domain (Notenboom et al., 2001); (15) 1D7B, cytochrome domain (Hallberg et al., 2000); (16) 2H1P (Young et al., 1997).
[b] Letters c - c mean that both MGD have a closed pyran ring, whereas c - o stands for one ring closed and the other open.

the β subunit and the ferredoxin is demonstrated by the superposition shown in Figure 5B. Notably, FS4 is a [3Fe-4S] cluster held by only three cysteines as in the seven-iron-type ferredoxin. The close similarity of the polypeptides curling around the clusters may have a physical background. A closer inspection shows that the observed peptide conformation causes an exceptionally large number of amides to point to the clusters, stabilizing their net negative charges.

Similar to the α subunit of EBDH, the chainfold of the β subunit resembles that of the β subunit of the respiratory nitrate reductase NarH (Bertero et al., 2003; Jormakka et al., 2004). The two chains show 290 structurally equivalent Cα atoms within the usual 3 Å cut-off criterion (Table 2). The equivalenced part has 46% sequence identity and the cluster positions deviate by less than 0.5 Å, indicating a close relationship. In both enzymes, all iron atoms of the four clusters are ligated by cysteines and the residues along the electron pathway are well conserved. Accordingly, the redox potential midpoints of these four clusters of EBDH should be similar to those of NarH. The β subunits of the pyrogallol-phloroglucinol transhydroxylase (Messerschmidt et al., 2004) and of two formate dehydrogenases (Jormakka et al., 2002; Raaijmakers et al., 2002) are more distantly related to those of EBDH (Table 2).

The γ Subunit

The γ subunit consists of 214 residues in a single domain forming a mostly antiparallel β sheet sandwich. All residues assume a defined conformation. The sheets form a crescent-like structure that envelops a noncovalently bound heme b (Figure 4C). The heme is well enclosed by the four large loops of residues 34–52, 98–115, 130–140, and 190–201, except for its two propionate side chains that make hydrogen bonds with Lys185-Nζ and

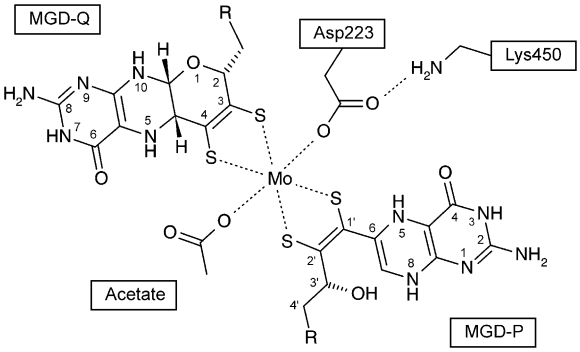

Figure 2. The Chemical Structure of the Observed Cofactor Mo-*bis*MGD

The numbering follows the relevant literature (Fischer et al., 1998). It is noteworthy that MGD-P has an open pyran ring as in the equivalent MGD reported for one of the two NarG structures (Table 2). In contrast, MGD-Q is closed. Its two stereo centers at positions 4a and 10a are both in the R configuration. The observed fifth (Asp223-Oδ2) and sixth (acetate) ligand of Mo are given. It should be noted that the exact structure of the piperazine ring of the open MGD-P cannot be derived from our electron density. It is conceivable that the piperazine ring is further oxidized by the nearby Mo redox center to an aromatic system.

His187-Nε of the β subunit. Heme b is tightly packed in its binding pocket, leaving no room for any other molecules.

In the crystal, the heme is planar and the iron lies exactly in the plane of the four pyrrole rings. The two axial ligands are Met108-Sδ with an Fe-S distance of 2.3 Å and Lys201-Nζ with an Fe-N distance of 2.0 Å. Its midpoint redox potential is +254 mV (B. Blaum and T. Friedrich, personal communication). The high potential can be explained by the nonpolar heme binding pocket and the two axial ligands favoring the uncharged ferrous heme over the charged ferric form. A search through the Protein Data Bank showed no other cases of heme proteins with axial methionine and lysine ligands. However, sequence alignments indicated that these ligands are most likely also present in the homologous enzymes DMS dehydrogenase (McDevitt et al., 2002), selenate reductase (Schröder et al., 1997), and chlorate reductase (Thorell et al., 2003). In comparison, the heme of formate dehydrogenase-N (Jormakka et al., 2002) has Met-Sδ and His-Nδ atoms as axial ligands and shows a midpoint potential of +169 mV. The lower midpoint potential with respect to the heme of EBDH agrees with the lower nucleophilicity of lysine in relation to histidine, diminishing the stabilization of the Fe^{3+} state.

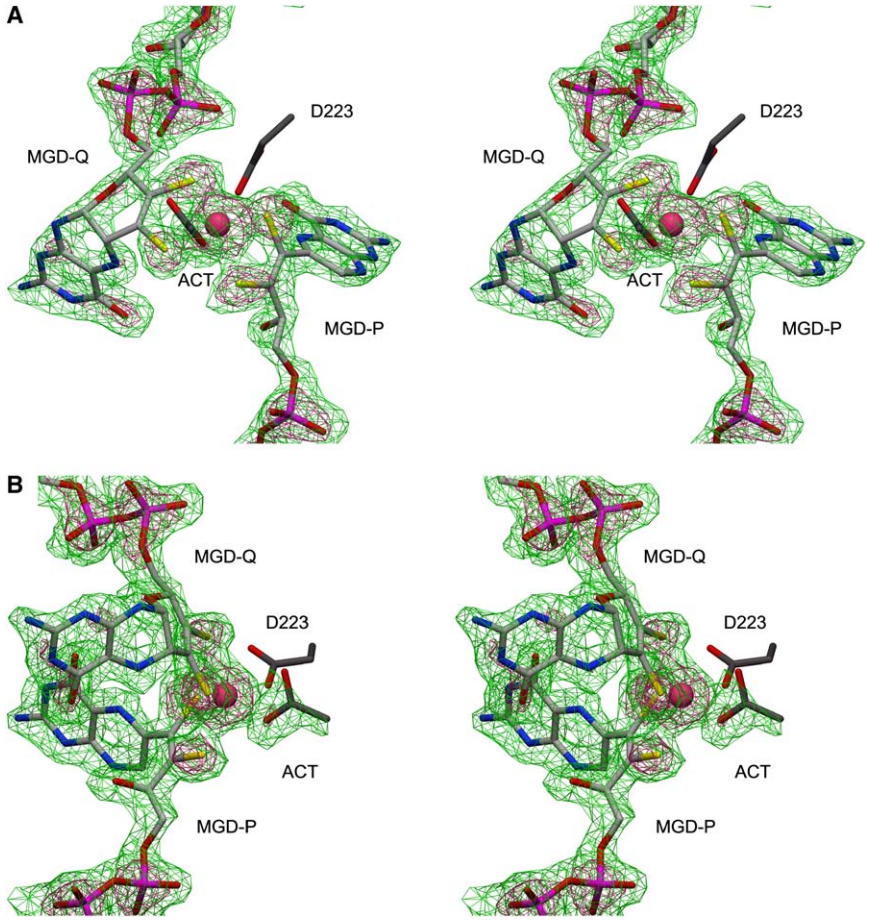

Figure 3. Structure of the Active Center around the Molybdenum Ion with the Original (Fo-Fc)-Difference Electron Density Obtained before Any Ligands Were Included in the Refinement

The density contour levels are at 2.5 σ (green) and 5.0 σ (pink). The density is not consistent with an oxo group at the Mo ion, indicating that molybdenum is in the reduced Mo(IV) state. (A) Standard view of the molybdenum center. (B) View rotated by 90° around a horizontal line to show the acetate in its original density. On refinement, acetate is completely covered by density and identified as such.

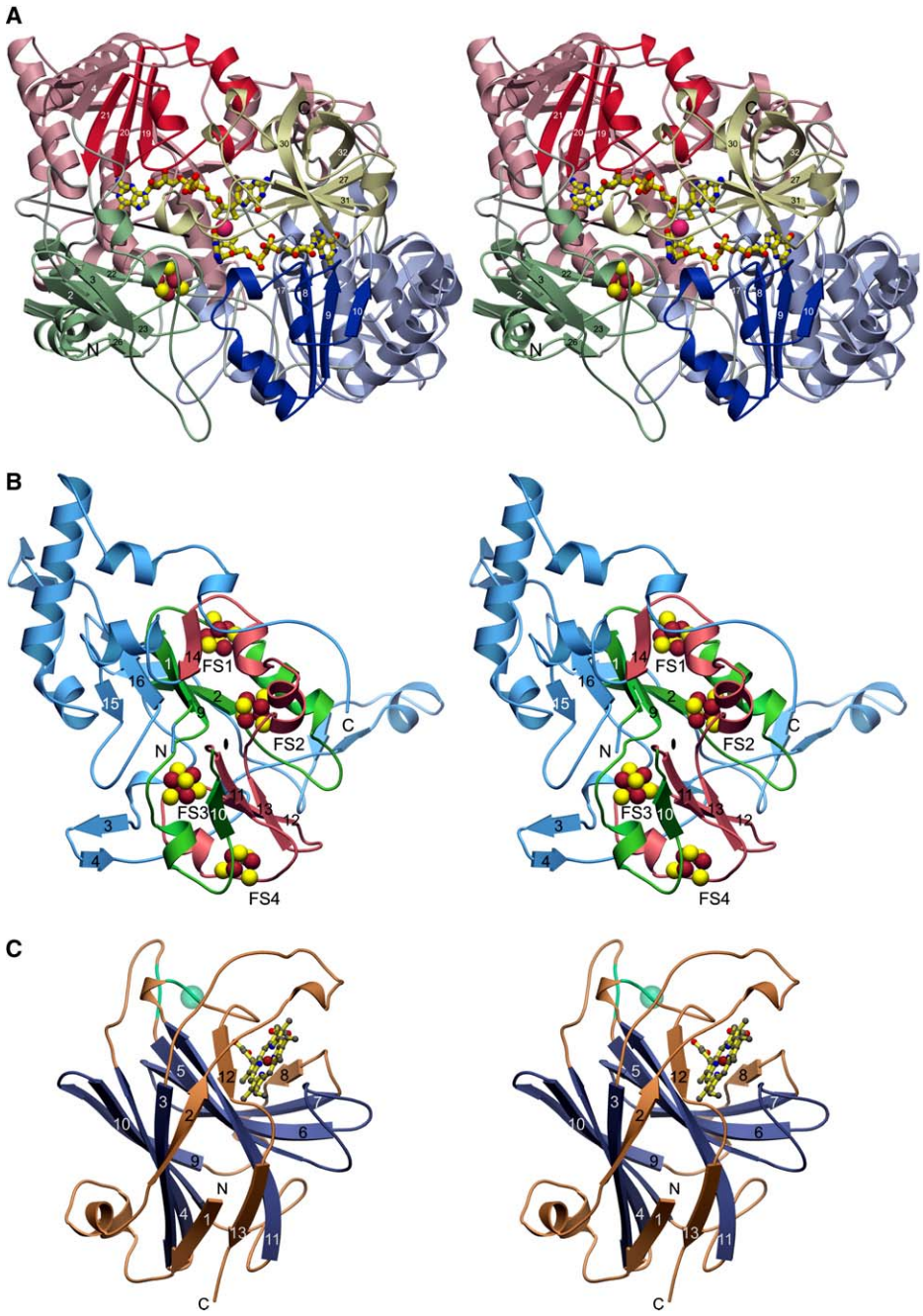

Figure 4. Explosion View of EBDH

The stereo ribbon plots are slightly reoriented in relation to Figure 1. In order to facilitate chain tracing, the sequential numbers of the β strands are given wherever possible. (A) The α subunit with Mo-*bis*MGD and iron sulfur cluster FS0. The active center pocket is indicated by a black line. The chain regions designated as domains I through IV in previous publications of DMSO family members (Boyington et al., 1997; Schindelin et al., 1996) are colored green, red, blue, and yellow, respectively. The segments constituting the domains are spatially close together but scattered along the chain. The Rossmann-type βαβαβ motifs binding the two guanine moieties of Mo-*bis*MGD are emphasized with dark colors. (B) The β subunit with its iron-sulfur clusters. The four clusters are bound to a pair of ferredoxin-like motifs. The green ferredoxin is N-terminal and followed by a duplication (red) related through a pseudo 2-fold axis (marked). The two parts are closely intertwined by a swap of strands β10 and β14 together with their preceding peptides. The additional polypeptide is colored blue. (C) The γ subunit with heme b. The chainfold resembles that of the V_H domain of antibodies (Table 2). The equivalenced chain parts are emphasized in dark blue. The location of the antigen binding site in relation to the V_H domain is indicated by green chain segments and a green sphere.

A search for structural homologs showed that the γ subunit is related to the carbohydrate binding domain C2 of a xylanase (Notenboom et al., 2001), to the cytochrome domain of an extracellular flavocytochrome cellobiose dehydrogenase (Hallberg et al., 2000), and more distantly to the V_H domain of antibodies (Table 2). The heme b position corresponds closely to the substrate binding site of the xylanase and to the heme binding site of the dehydrogenase. In view of the well-matching cofactor and substrate binding sites, the

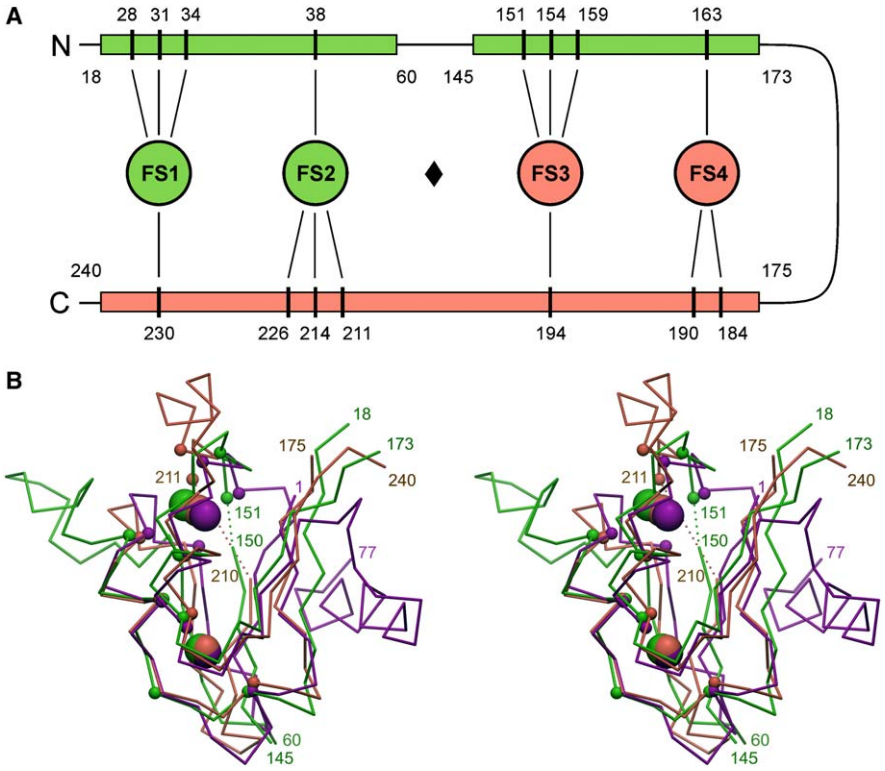

Figure 5. Relationship between the β Subunit and Ferredoxin

(A) Sketch of the β subunit with the colors of Figure 4B. The β subunit can be considered as two copies of a ferredoxin in tandem along the chain with swapped parts (Figure 4B), a large insertion after position 60, and 112 additional residues after position 240.

(B) Stereoview of a seven-iron-type ferredoxin (Macedo-Ribeiro et al., 2001) drawn in purple with chain segments of the β subunit colored as in Figure 4B. The chain superposition brings the iron-sulfur clusters (large spheres, FS2 and FS3 at the top, FS1 and FS4 at the bottom) close together. The same applies for the cysteines holding the clusters, the Cα atoms of which are indicated by small spheres. Note that the superposition is over the pseudo 2-fold axis so that the swap connection 210-211 does not exactly fit. The other swap connection 150-151 fits well.

xylanase and the dehydrogenase seem to be related through evolution. Interestingly, the antigen binding site of the V_H domain marked in Figure 4C is in an adjacent position when related to the β sheet sandwich. However, the relationship with the V_H domain is more distant and may be of a physical rather than evolutionary nature.

Active Center and Catalysis

The active center of EBDH is defined by the molybdenum ion, which can be reached through the 25 Å long tunnel-shaped pocket lined by mostly nonpolar residues. The molybdenum ion is coordinated by six ligands in a slightly distorted trigonal prismatic geometry (Figure 6). Four of the ligands are the *cis*-dithiolene sulfur atoms of the two MGD molecules located at distances between 2.3 Å and 2.5 Å. The fifth and sixth coordination sites are occupied by Asp223-Oδ2 and by an oxygen atom of a bound acetate ion from the buffer at distances of 2.0 Å and 2.4 Å, respectively. The side chain of Asp223 is held in place by Lys450-Nζ backed up by the carbonyl oxygens of residues 222 and 446. The same Asp-Lys pair is conserved in selenate reductase (Schröder et al., 1997) and in chlorate reductase (Thorell et al., 2003), whereas it is an Asp-Arg pair in DMS dehydrogenase (McDevitt et al., 2002). These interactions cause Asp223 to act as a monodentate ligand to Mo. A monodentate aspartate ligand was also observed in one of the two NarG structures, whereas a bidentate aspartate coordination was found in the other (Table 2).

In the analyzed EBDH crystal, the molybdenum ion has no attached oxo group (Figure 3), indicating that it is in the reduced Mo(IV) state. In order to outline the geometry of the catalytic reaction, a product molecule was modeled into the active center (Figure 6). This model suggests the reaction sequence shown in Figure 7A. It is supported by enzyme activity and inhibition data of several substrate-related compounds given in Figure 7B. These compounds outline the active center pocket and their relative catalytic rates support the suggested reaction geometry.

Electron Transport

After the hydroxylation of ethylbenzene, the molybdenum ion is in the Mo(IV) state and must be reoxidized to Mo(VI) in order to complete the reaction cycle. This is achieved through the chain of redox cofactors connecting the molybdenum with heme b of the γ subunit, from where the electrons are donated to a yet-unknown carrier. Presumably, this carrier is a cytochrome c, coupling ethylbenzene oxidation to the nitrate respiration of *A. aromaticum*. The structure of the electron transport chain is shown in Figure 8.

The electron transport chain starts with a comparatively long edge-to-edge distance of 8.4 Å between the S4α atom of MGD-Q at Mo(IV) and Cys86-Sγ at cluster

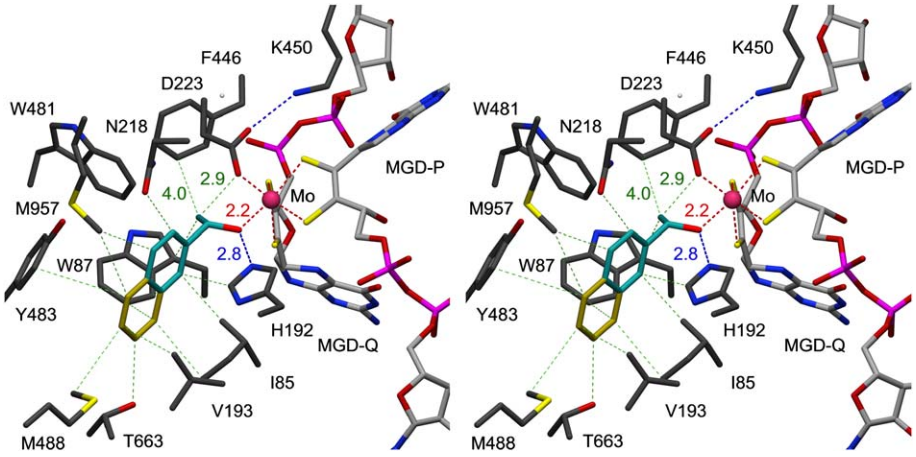

Figure 6. Stereoview of the Active Center Showing the Position of the Modeled Reaction Product 1-(*S*)-Phenylethanol in Cyan and, after the Addition of the Second Phenyl Ring Colored Yellow, also the Position of the Product 1-(*S*)-(2′-Naphthyl)Ethanol

The contacts (green dashed lines) indicate distances larger than 3.2 Å. Four distances are specified. The addition of the second phenyl ring causes only a negligible change of the ethanol conformation and position, demonstrating how substrates larger than the usual ethylbenzene can be accommodated. The molybdenum ion shows a slightly distorted trigonal prismatic coordination. Both the open molybdopterin cofactor MGD-P and the closed cofactor MGD-Q serve as bidentate ligands via their dithiolene sulfurs. The fifth ligand is Asp223-Oδ2 backed up by Lys450-Nζ. During catalysis, His192 is expected to function as a base. The observed *S*-configuration of the reaction product is consistent with the active center geometry.

FS0. Here, a through-bond combined with a 4.0 Å through-space transfer from the C4a or N10 atoms of MGD-Q to Cys86-Cα seems possible (Figure 8). Cluster FS0 is unusual in that one of the four iron ligands is a histidine instead of a cysteine as commonly observed. Such a [4Fe-4S] cluster environment has only been found in nitrate reductase NarG (Bertero et al., 2003; Jormakka et al., 2004), in a hydrogenase (Volbeda et al., 1995), and in the Rieske protein component of cytochrome bc1 (Iwata et al., 1996). Moreover, Lys129-Nζ is hydrogen bonded to N8α of MGD-Q and at a close 3.9 Å distance to Cys127-Sγ at FS0. A lysine or arginine was also observed at the equivalent positions of NarG (Bertero et al., 2003), of formate dehydrogenases-N (Jormakka et al., 2002) and -H (Boyington et al., 1997), of the nitrate reductase NapA (Dias et al., 1999; Arnoux et al., 2003), and of arsenite oxidase (Ellis et al., 2001). This residue is probably important because a change from lysine to methionine in NapA from *Ralstonia eutropha* inactivated the enzyme completely (Hettmann et al., 2003). The histidine ligand and the adjacent lysine point to a relatively high midpoint potential of FS0.

In each of the following transfer steps from FS0 to FS4, two of the four cysteines attached to each cluster are close together, reminiscent of the relationship between the two clusters of the ferredoxins (Figure 5). All distances are short so that the transfer should be much faster than the chemical reactions (Page et al., 1999). The last step from the [3Fe-4S] cluster FS4 to the heme has the longest edge-to-edge distance. However, there are through-bond pathways along the hydrogen bonds between Lys185 and His187 of the β subunit and the two propionate groups of the heme, as well as through Cys163 and Pro164-Cδ via a 4.0 Å through-space distance to the 1-carbon of a propionate (Figure 8). An addition of the six through-space transfer distances results in 43.6 Å, which is 20.4 Å shorter than the direct through-space distance of 64.0 Å between the molybdenum and the heme iron.

Discussion

Catalytic Mechanism

While all other structurally known Mo-*bis*MGD enzymes process polar substrates, EBDH hydroxylates an inert hydrocarbon molecule. In the presented crystal structure, the molybdenum is presumably in its Mo(IV) state because the alternative Mo(VI) state would bind a water

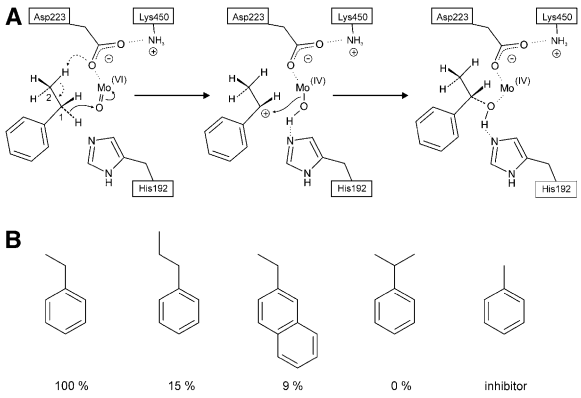

Figure 7. Putative Reaction Sequence of EBDH

(A) Sketch of the catalytic reaction starting from an oxo group bound to the Mo(VI) ion. The C2 atom is polarized by Asp223-Oδ2 backed-up by Lys450-Nζ facilitating the flow of an electron pair and a proton from the C1 atom to the oxo group at Mo(VI). Subsequently, the transient carbocation accepts the hydroxyl group leaving molybdenum in its reduced Mo(IV) state. Most likely, His192-Nε supports the transfer in both directions. After transferring the two electrons via heme b to the external acceptor, the resulting Mo(VI) binds a water molecule at the position of one of the oxygens of the acetate (Figure 3) and converts it to an oxo group (not shown). The two emerging protons can be picked up by His192 and released through the active center pocket to the bulk solvent.

(B) Relative enzyme activities for the five related molecules ethylbenzene, *n*-propylbenzene, 2′-ethylnaphthalene, *iso*-propylbenzene (is not an inhibitor), and toluene. The specific activity of EBDH for ethylbenzene is 1.9 U/mg.

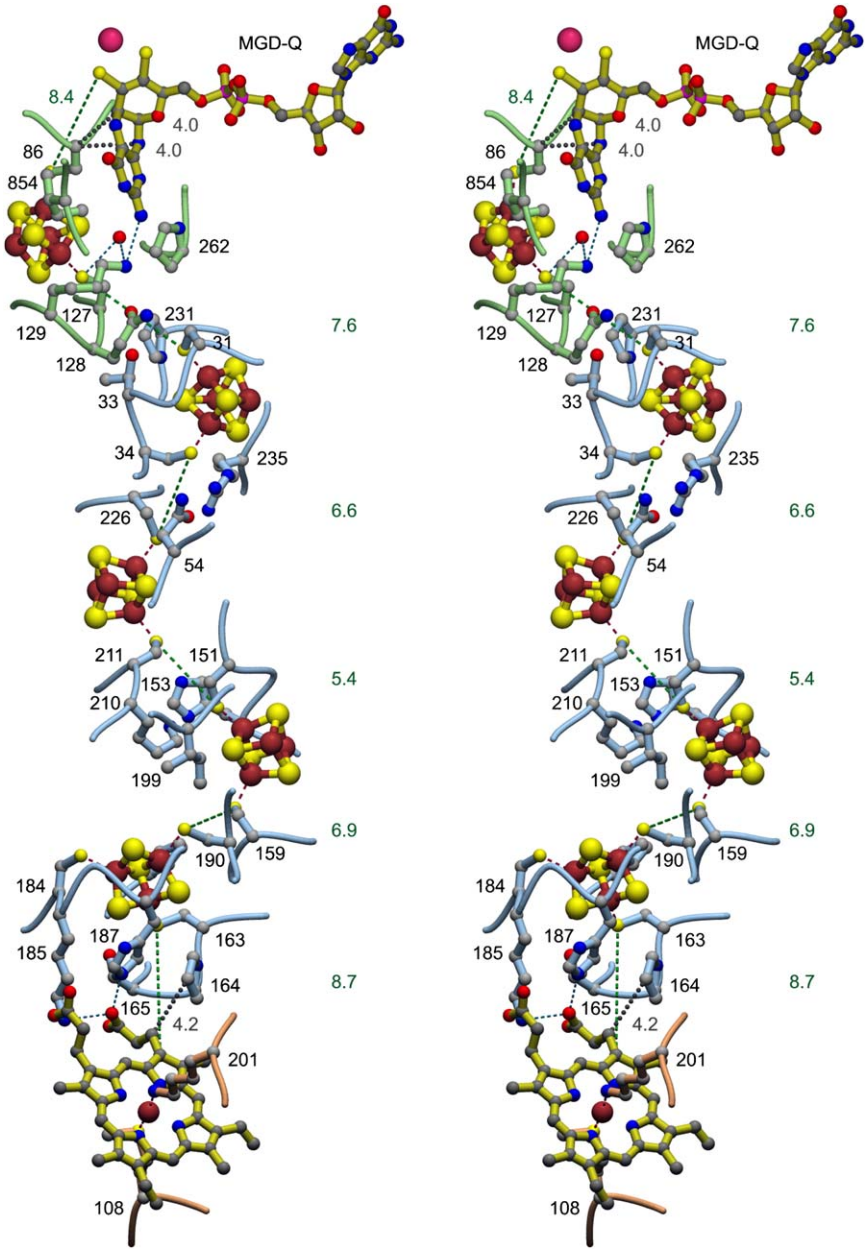

Figure 8. Stereoview of the Electron Transport Chain between the Molybdenum Ion and Heme b

All residues are given in their subunit colors (Figure 1). The axial ligands of the heme iron are a methionine and a lysine. Lys185 and His187 of the β subunit are in close proximity to the [3Fe-4S] cluster FS4 and directly hydrogen bonded to the heme propionate side chains. The edge-to-edge distances of the redox factors, which extend between the thiol groups at Mo, the cysteine $S\gamma$ atoms holding the clusters, and the porphyrin ring are indicated by green dashed lines. Hydrogen bonds are shown as blue dashed lines and the 4.0 Å and 4.2 Å through-space transfer routes by gray dotted lines.

molecule and convert it to an oxo ligand. Certainly no such ligand is present as demonstrated by the electron density shown in Figure 3. The crystal structure corresponds to the resting state after hydroxylation has occurred and should be able to accommodate the reaction product 1-(*S*)-phenylethanol. Therefore, we modeled this complex placing the hydroxyl group in the position of the buffer acetate oxygen coordinating Mo(IV). As shown in Figure 6 the product fits well into the active center pocket. The side chains of Trp87 and Trp481 on one side and the Mo-coordinating Asp223 on the other hold the phenyl ring in place and provide enough space for the 2-methyl group, which contacts Phe446.

The proposed reaction sequence starts with an oxidation of the Mo(IV) ion to the Mo(VI) state by the removal of two electrons via the electron transport chain to the heme. Mo(VI) binds a water molecule, most likely at the position where the acetate oxygen contacts the molybdenum ion in our structure (Figure 6) as no suitably positioned water molecule was present. The Mo(VI)-water adduct releases two protons via His192 to the bulk solvent to form the oxo group shown as the initial state

in Figure 7A. After substrate binding, the C2 atom is polarized by the carboxyl group of Asp223, supporting the transfer of an electron pair and a proton from the C1 atom to the oxo group at Mo(VI). This transfer results in a transient hydroxyl group bound to Mo(IV) and in a transient carbocation at C1. Subsequently, the hydroxyl group at Mo(IV) adds to the C1 atom of the substrate. His192-Nε most likely facilitates the transfer in both directions. The observed geometry is consistent with this proposal but cannot confirm it in detail. However, it is clear that the C2 atom is required for catalysis because toluene is not hydroxylated and known to act as an inhibitor, although the C1 atom should be at the appropriate position. Moreover, the formation of a transient carbocation instead of a C1-C2 double bond is supported by the inability of the enzyme to process styrene (Johnson and Spormann, 1999).

As shown in the model of Figure 6, the substrate ethylbenzene fits perfectly into the end of the active center pocket at the molybdenum ion. The activity data of ethylbenzene and closely related compounds (Figure 7B) indicate that there is some space left in front of the C2 atom because EBDH is still active with *n*-propylbenzene. This agrees well with the rather long distance between C2 and Phe446. However, there is no space around the C1 atom as *iso*-propylbenzene is inactive and does not even bind. The relatively high activity of EBDH for 2′-ethylnaphthalene demonstrates that there is enough space on the side of the substrate facing the opening of the active center pocket (Figure 6). The fact that toluene apparently binds well but is not processed agrees with the structure and also with the proposed reaction sequence, which requires the C2 atom for the deprotonation of C1 (Figure 7A).

Structure-Based Comparisons

The three subunits of EBDH differ greatly from each other. The α subunit with its Mo-*bis*MGD cofactors shows chainfold similarity and also some sequence similarity to the other structurally established enzymes of the DMSO family listed in Table 2. The closest relative is certainly the respiratory nitrate reductase subunit NarG, which, however, has a more than 300 residue longer chain. Both are the only structurally known members of subfamily II, which is defined by an aspartate as Mo ligand. Moreover, NarG also has an open MGD in common with EBDH.

It should be noted that the electron flow direction of NarGHI and EBDH are reversed, although the transfer pathways are structurally very similar. In EBDH, the substrate is anaerobically oxidized in the α subunit and the resulting two electrons pass over to the heme of the γ subunit, where they are probably picked up by a soluble cytochrome. In contrast, the hemes of the γ' subunit of NarGHI from *E. coli*, which are located in the membrane, pick up electrons from the quinone pool and transfer them to the α subunit where they reduce nitrate to nitrite. This indicates that the β subunit should merely function as a conducting wire implying similar redox potentials for all four clusters. A third possibility is observed in the homologous β subunit of pyrogallol-phloroglucinol transhydroxylase, which lacks the fourth cluster (Table 2). Presumably, this enzyme uses the clusters as a short-term electron sink rather than for electron transfer (Messerschmidt et al., 2004).

Some DMSO family members share a similar β subunit with EBDH (Table 2). Again the closest relative is the respiratory nitrate reductase subunit NarH, despite its approximately 150 additional residues. In contrast, the γ subunit of EBDH has no counterpart in the structurally known DMSO family members. However, with respect to chainfold and active center locations, it is related to structurally distinct domains of otherwise completely unrelated proteins (Table 2).

NarGHI of *E. coli* and EBDH are in different cellular locations. EBDH is soluble in the periplasm, whereas NarGHI of *E. coli* is located in the cytoplasm but attached to the cytoplasmic membrane through its membrane-immersed γ' subunit. In contrast to NarGHI of *E. coli*, the NarGHI enzymes of extreme halo- and thermophile archaea are located outside the cytoplasm, but they are not soluble like EBDH. Most likely, these archaeal NarGHI are attached to the cytoplasmic membrane through a presumably α-helical *trans*-membrane anchor at the C terminus of their γ' subunits.

Experimental Procedures

Protein Production and Enzymatic Assay

A. aromaticum strain EbN1 was cultivated anaerobically in 1 l stoppered bottles in mineral salt medium at 30°C with ethylbenzene (1 mM) as the carbon and energy source and nitrate (10 mM initial concentration) as terminal electron acceptor (Rabus and Widdel, 1995). Subsequently, bacteria were grown anaerobically in a 200 l batch and harvested as described (Kniemeyer and Heider, 2001; Rabus and Heider, 1998). For enzyme preparation, 40 g of wet cells were resuspended in 40 ml of a 20% (v/v) aqueous glycerol solution containing 0.05 mg/ml DNAase I (Applichem). Cells were passed once through a French press (137 MPa), and cellular debris was removed by ultracentrifugation for 1 hr at 4°C at 100,000 × g. EBDH was stabilized by adding 100 μM of the oxidant ferricenium tetrafluoroborate (Aldrich).

All chromatographic steps were carried out over a period of 4 days under aerobic conditions at 4°C. Cell extracts were applied on a Q-Sepharose fast flow column (Amersham Biosciences) equilibrated with buffer A (10 mM Tris-HCl [pH 8.0], 10% glycerol, and 100 μM ferricenium tetrafluoroborate). EBDH was in the flow through, which was then centrifuged (1 hr, 4°C, 100,000 × g) to remove particulate material. The supernatant was loaded onto a ceramic hydroxylapatite column (Bio-Rad) equilibrated with buffer B (10 mM Tris-acetate [pH 8.0], 10% glycerol, and 10 μM ferricenium tetrafluoroborate). By using a 0–300 mM potassium phosphate gradient in buffer A, EBDH eluted between 160 and 200 mM potassium phosphate and was pure by SDS gel electrophoresis. The procedure resulted in 1.5 mg EBDH per gram of wet cell mass.

The catalytic activity of EBDH was measured as the decrease of absorption of ferricenium at 290 nm as previously described (Kniemeyer and Heider, 2001), except that the assay was performed at the optimum temperature of EBDH of 55°C and that 100 μM ferricenium tetrafluoroborate (Aldrich) was used as electron acceptor instead of ferricenium hexafluorophosphate.

Crystallization, Data Collection, and Phasing

EBDH was crystallized in sitting drops under strictly anaerobic conditions in a glove box at 293 K. A drop consisted of 2.5 μl protein solution (21 mg/ml EBDH, 10 mM Tris-acetate [pH 8.0], 160 mM potassium phosphate, 10% glycerol, 100 μM ferricenium tetrafluoroborate) and 2.5 μl reservoir buffer (45%–50% PEG 550 MME, 125 mM MES [pH 6.5], 3.5 mM $ZnSO_4$). It should be expected that the oxidant in the drop was consumed after a couple of hours so that the crystalline enzyme should be in its reduced state. Crystals appeared after a few days and reached their maximum size of 100 × 100 × 500 μm^3 within four weeks. Due to the arid conditions

in the glove box, the evaporation of the reservoir solution was significant, increasing the precipitant concentration to levels sufficient for cryoprotection. In an aerobic environment, the crystals lost their red color within about 8 hr, presumably because the heme iron was oxidized. The crystals also lost their diffraction power, probably because of damage by oxygen radicals produced by the reduced heme iron. However, the EBDH crystals were stable when flash frozen in liquid nitrogen directly after removal from the glove box.

All data were collected at beam line X06SA at the Swiss Light Source (Villigen, CH). The SAD data set was collected at the iron K edge with a strongly attenuated beam. The K edge had been determined by an X-ray fluorescence scan. All diffraction intensities were processed and scaled with XDS and XSCALE (Kabsch, 1993). The anomalous differences were calculated with XPREP (Bruker Nonius) and the positions of five Fe-S clusters and of the heme b iron were established with SHELXD (Schneider and Sheldrick, 2002). However, the individual iron atoms within the clusters were not resolved so that the five clusters had to be treated as single entities. Accordingly, the protein phases were calculated to merely 4.2 Å resolution with MLPHARE (Otwinowski, 1991). Density modification with RESOLVE (Terwilliger, 2000) resulted in an interpretable map at 4.2 Å resolution. Following the Fe-S cluster positions, which were clearly established by the anomalous signal, several polypeptide chain segments of the homologous α and β subunits of the *E. coli* respiratory nitrate reductase NarGHI (Bertero et al., 2003) were placed manually into the electron density by using COOT (Emsley and Cowtan, 2004). The model phases from this partial model of the EBDH α and β subunits was combined with the SAD phases by using RESOLVE and, in numerous iterative steps, extended to 2.4 Å resolution. The resulting electron density map was manually traced with COOT yielding a 90% complete model. At the final stages of the phasing procedure, the phases were extended to 1.88 Å resolution with the high-resolution data set, and model building was continued with ARP/wARP (Perrakis et al., 1999).

Structure Refinement and Modeling

The model was completed by rounds of manual rebuilding with COOT and refinement with REFMAC (Murshudov et al., 1997). All cofactors were clearly visible in difference Fourier maps and included in the model. Water molecules were placed with ARP/wARP and manually checked for good stereochemistry. Finally the structure was refined with one TLS group for each subunit with its cofactors. No restraints were applied to metal-ligand distances at the Mo center. For modeling of substrate and product complexes, ligands were manually placed into the active center cavity by using COOT and then energy minimized with CNS (Brünger et al., 1998). Coordinates and topology of cofactors and ligands were generated and energy minimized by using PRODRG2 (Schüttelkopf and van Aalten, 2004). Structure similarity searches were performed with DALI (Holm and Sander, 1993), superpositions produced with SSM (Krissinel and Henrick, 2004), and structure-based sequence alignments with T-COFFEE (Poirot et al., 2004). Figures were generated with POVscript+ (Fenn et al., 2003) and POVRAY (http://www.povray.org/).

Acknowledgments

We thank the team of the Swiss Light Source for their support during data collection. The work was supported by the Deutsche Forschungsgemeinschaft under grants SFB388 and HE2190/4.

Received: April 3, 2006
Revised: June 16, 2006
Accepted: July 3, 2006
Published: September 12, 2006

References

Arnoux, P., Sabaty, M., Alric, J., Frangioni, B., Giogliarelli, B., Adriano, J.-M., and Pignol, D. (2003). Structural and redox plasticity in the heterodimeric periplasmatic nitrate reductase. Nat. Struct. Biol. *10*, 928–934.

Bertero, M.G., Rothery, R.A., Palak, M., Hou, C., Lim, D., Blasco, F., Weiner, J.H., and Strynadka, N.C.J. (2003). Insights into the respiratory electron transfer pathway from the structure of nitrate reductase A. Nat. Struct. Biol. *10*, 681–687.

Boyington, J.C., Gladyshev, V.N., Khangulov, S.V., Stadtman, T.C., and Sun, P.D. (1997). Crystal structure of formate dehydrogenase H: catalysis involving Mo, molybdopterin, selenocysteine, and an Fe_4S_4 cluster. Science *275*, 1305–1308.

Brünger, A.T., Adams, P.D., Clore, G.M., DeLano, W.L., Gros, P., Grosse-Kunstleve, R.W., Jiang, J.S., Kuszewski, J., Nilges, M., Pannu, N.S., et al. (1998). Crystallography & NMR system: a new software suite for macromolecular structure determination. Acta Crystallogr. D Biol. Crystallogr. *54*, 905–921.

Czjzek, M., Dos Santos, J.-P., Pommier, J., Giordano, G., Mejean, V., and Haser, R. (1998). Crystal structure of oxidized trimethylamine *N*-oxide reductase from *Shewanella massilia* at 2.5 Å resolution. J. Mol. Biol. *284*, 435–447.

Dias, J.M., Than, M.E., Humm, A., Huber, R., Bourenkov, G.P., Bartunik, H.D., Bursakov, S., Calvete, J., Caldeira, J., Carneiro, C., et al. (1999). Crystal structure of the first dissimilatory nitrate reductase at 1.9 Å solved by MAD methods. Structure *7*, 65–79.

Ellis, P.J., Conrads, T., Hille, R., and Kuhn, P. (2001). Crystal structure of the 100 kDa arsenite oxidase from *Alcaligenes faecalis* in two crystal forms at 1.64 Å and 2.03 Å. Structure *9*, 125–132.

Emsley, P., and Cowtan, K. (2004). Coot: Model-building tools for molecular graphics. Acta Crystallogr. D Biol. Crystallogr. *60*, 2126–2132.

Fenn, T.D., Ringe, D., and Petsko, G.A. (2003). POVScript+: A program for model and data visualization using persistence of vision ray-tracing. J. Appl. Crystallogr. *36*, 944–947.

Fischer, B., Enemark, J.H., and Basu, P. (1998). A chemical approach to systematically designate the pyranopterin centers of molybdenum and tungsten enzymes and synthetic models. J. Inorg. Biochem. *72*, 13–21.

Hallberg, B.M., Bergfors, T., Bäckbro, K., Pettersson, G., Henriksson, G., and Divne, C. (2000). A new scaffold for binding haem in the cytochrome domain of the extracellular flavocytochrome cellobiose dehydrogenase. Structure *8*, 79–88.

Hettmann, T., Siddiqui, R.A., von Langen, J., Frey, C., Romao, M.J., and Diekmann, S. (2003). Mutagenesis study on the role of a lysine residue highly conserved in formate dehydrogenases and periplasmic nitrate reductases. Biochem. Biophys. Res. Commun. *310*, 40–47.

Hille, R. (1996). The mononuclear molybdenum enzymes. Chem. Rev. *96*, 2757–2816.

Hille, R. (2002). Molybdenum and tungsten in biology. Trends Biochem. Sci. *27*, 360–367.

Holm, L., and Sander, C. (1993). Protein structure comparison by alignment of distance matrices. J. Mol. Biol. *233*, 123–138.

Iwata, S., Saynovits, M., Link, T.A., and Michel, H. (1996). Structure of a water soluble fragment of the 'Rieske' iron-sulfur protein of the bovine heart mitochondrial cytochrome bc1 complex determined by MAD phasing at 1.5 Å resolution. Structure *4*, 567–579.

Johnson, H.A., and Spormann, M.A. (1999). In vitro studies on the initial reactions of anaerobic ethylbenzene mineralization. J. Bacteriol. *181*, 5662–5668.

Johnson, H.A., Pelletier, D.A., and Spormann, A.M. (2001). Isolation and characterization of anaerobic ethylbenzene dehydrogenase, a novel Mo-Fe-S enzyme. J. Bacteriol. *183*, 4536–4542.

Jormakka, M., Törnroth, S., Byrne, B., and Iwata, S. (2002). Molecular basis of proton motive force generation: structure of formate dehydrogenase-N. Science *295*, 1863–1868.

Jormakka, M., Richardson, D., Byrne, B., and Iwata, S. (2004). Architecture of NarGH reveals a structural classification of Mo-*bis*MGD enzymes. Structure *12*, 95–104.

Kabsch, W. (1993). Automatic processing of rotation diffraction data from crystals of initially unknown symmetry and cell constants. J. Appl. Crystallogr. *26*, 795–800.

Kniemeyer, O., and Heider, J. (2001). Ethylbenzene dehydrogenase, a novel hydrocarbon-oxidizing molybdenum/iron-sulfur/heme enzyme. J. Biol. Chem. *276*, 21381–21386.

Krissinel, E., and Henrick, K. (2004). Secondary-structure matching (SSM), a new tool for fast protein structure alignment in three dimensions. Acta Crystallogr. D Biol. Crystallogr. *60*, 2256–2268.

Macedo-Ribeiro, S., Martins, B.M., Pereira, P.J.B., Buse, G., Huber, R., and Soulimane, T. (2001). New insights into the thermostability of bacterial ferredoxins: high-resolution crystal structure of the seven-iron ferredoxin from *Thermus thermophilus*. J. Biol. Inorg. Chem. *6*, 663–674.

McAlpine, A.S., McEwan, A.G., and Bailey, S. (1998). The high resolution crystal structure of DMSO reductase in complex with DMSO. J. Mol. Biol. *275*, 613–623.

McDevitt, C.A., Hugenholtz, P., Hanson, G.R., and McEwan, A.G. (2002). Molecular analysis of dimethyl sulphide dehydrogenase from *Rhodovulum sulfidophilum*: its place in the dimethyl sulphoxide reductase family of microbial molybdopterin-containing enzymes. Mol. Microbiol. *44*, 1575–1587.

Messerschmidt, A., Niessen, H., Abt, D., Einsle, O., Schink, B., and Kroneck, P.M.H. (2004). Crystal structure of pyrogallol-phloroglucinol transhydroxylase, an Mo enzyme capable of intermolecular hydroxyl transfer between phenols. Proc. Natl. Acad. Sci. USA *101*, 11571–11576.

Murshudov, G.N., Vagin, A.A., and Dodson, E.J. (1997). Refinement of macromolecular structures by the maximum-likelihood method. Acta Crystallogr. D Biol. Crystallogr. *53*, 240–255.

Notenboom, V., Boraston, A.B., Kilburn, D.G., and Rose, D.R. (2001). Crystal structures of the family 9 carbohydrate-binding module from *Thermotoga maritima* xylanase 10A in native and ligand-bound forms. Biochemistry *40*, 6248–6256.

Otwinowski, Z. (1991). Isomorphous replacement and anomalous scattering. In Proceedings of the CCP4 Study Weekend, W. Wolf, P.R. Evans, and A.G.W. Leslie, eds. (Warrington, UK: Daresbury Laboratory), pp. 80–86.

Perrakis, A., Morris, R., and Lamzin, V.S. (1999). Automated protein model building combined with iterative structure refinement. Nat. Struct. Biol. *6*, 458–463.

Page, C.C., Moser, C.C., Chen, X., and Dutton, P.L. (1999). Natural engineering principles of electron tunnelling in biological oxidation-reduction. Nature *402*, 47–52.

Poirot, O., Suhre, K., Abergel, C., O'Toole, E., and Notredame, C. (2004). 3DCoffee@igs: a web server for combining sequences and structures into a multiple sequence alignment. Nucleic Acids Res. *32*, W37–W40.

Raaijmakers, H., Macieira, S., Dias, J.M., Teixeira, S., Bursakov, S., Huber, R., Moura, J.J.G., Moura, I., and Romao, M.J. (2002). Gene sequence and the 1.8 Å crystal structure of the tungsten-containing formate dehydrogenase from *Desulfovibrio gigas*. Structure *10*, 1261–1272.

Rabus, R., and Widdel, F. (1995). Anaerobic degradation of ethylbenzene and other aromatic hydrocarbons by new denitrifying bacteria. Arch. Microbiol. *163*, 96–103.

Rabus, R., and Heider, J. (1998). Initial reactions of anaerobic metabolism of alkylbenzenes in denitrifying and sulfate-reducing bacteria. Arch. Microbiol. *170*, 377–384.

Rabus, R., Kube, M., Beck, A., Widdel, F., and Reinhardt, R. (2002). Genes involved in the anaerobic degradation of ethylbenzene in a denitrifying bacterium, strain EbN1. Arch. Microbiol. *178*, 506–516.

Schindelin, H., Kisker, C., Hilton, H., Rajagopalan, K.V., and Rees, D.C. (1996). Crystal structure of DMSO reductase: redox-linked changes in molybdopterin coordination. Science *272*, 1615–1621.

Schneider, F., Löwe, J., Huber, R., Schindelin, H., Kisker, C., and Knäblein, J. (1996). Crystal structure of dimethyl sulfoxide reductase from *Rhodobacter capsulatus* at 1.88 Å resolution. J. Mol. Biol. *263*, 53–69.

Schneider, T.R., and Sheldrick, G.M. (2002). Substructure solution with SHELXD. Acta Crystallogr. D Biol. Crystallogr. *58*, 1772–1779.

Schröder, I., Rech, S., Krafft, T., and Macy, J.M. (1997). Purification and characterization of the selenate reductase from *Thauera selenatis*. J. Biol. Chem. *272*, 23765–23768.

Schulz, G.E. (1992). Binding of nucleotides by proteins. Curr. Opin. Struct. Biol. *2*, 61–67.

Schüttelkopf, A.W., and van Aalten, D.M.F. (2004). PRODRG: a tool for high-throughput crystallography of protein-ligand complexes. Acta Crystallogr. D Biol. Crystallogr.D *60*, 1355–1363.

Szaleniec, M., Jobst, B., and Heider, J. (2003). Ethylbenzene dehydrogenase: oxidation of hydrocarbons without oxygen. Ann. Pol. Chem. Soc. *2003*, 240–245.

Terwilliger, T.C. (2000). Maximum likelihood density modification. Acta Crystallogr. D Biol. Crystallogr. *56*, 965–972.

Thorell, H.D., Stenklo, K., Karlsson, J., and Nilsson, T. (2003). A gene cluster for chlorate metabolism in *Ideonella dechloratans*. Appl. Environ. Microbiol. *69*, 5585–5592.

Volbeda, A., Charon, M.H., Piras, C., Hatchikian, E.C., Frey, M., and Fontecilla-Camps, J.C. (1995). Crystal structure of the nickel-iron hydrogenase from *Desulfovibrio gigas*. Nature *373*, 580–587.

Young, A.C.M., Valadon, P., Casadevall, A., Scharff, M.D., and Sacchettini, J.C. (1997). The three-dimensional structures of a polysaccharide binding antibody to *Cryptococcus neoformans* and its complex with a peptide from a phage display library: implications for the identification of peptide mimotopes. J. Mol. Biol. *274*, 622–634.

Accession Numbers

The coordinates and structure factors have been deposited in the Protein Data Bank under accession code 2IVF.